GSA Data Repository 2018322

Supplementary material for **"Large vertical displacements of a crystalline massif recorded by Raman thermometry"**

Section DR1: RSCM method

Raman Spectroscopy of Carbonaceous Material (RSCM) analysis was performed in situ on polished, uncovered thin sections at The Raman Laboratory of the Institute of Geological Sciences, University of Bern. A confocal notch filter-based Jobin-Yvon LabRAM HR800 spectrometer was used for spectrum acquisition. It is equipped with an Olympus BX41 100x confocal microscope, a Peltier-cooled CCD detector (Andor Technology) and an air-cooled Nd-YAG laser (Compass 315 M, coherent, 20 mW) having a beam spot of approximately 1 μm diameter and a wavelength of 532.12 nm. The software LabSpec 4.14 of HORIBA Jobin-Yvon was used to execute the measurements. At the beginning of each measurement series, a silicon

standard was used to check the calibration and signal intensity. Acquisition time varied between 20 and 120 seconds, depending on the signal to noise ratio and was divided into two to four accumulation cycles, in order to avoid artefacts. Raman spectra were acquired in the range of 500 to 2200 cm^{-1} so that both, base line and all necessary first order Raman bands of carbonaceous material (CM) can be recognized. 10 to 63 individual spots of CM per sample were analyzed, depending on (1) the number of suitable particles and (2) on the diversity of spectra observed during the first 10 measurements. Because it is located only a few decameters away from sample M73, only 3 measurements were performed on sample M67.

Thin sections were prepared and analyzed following the procedure described in Lünsdorf et al. (2014). The Raman spectrum of CM can vary as a function of the crystallographic orientation of the measured particle. To reduce this effect, thin sections were analyzed in the plane perpendicular to the main foliation and parallel to the stretching lineation whenever possible.

We used an automated, iterative and randomized approach for curve-fitting and temperature estimation, based on the Python script "Ifors" (Lünsdorf et al., 2014; Lünsdorf and Lünsdorf, 2016; Lünsdorf et al., 2017). This software has the following advantages: (1) it reduces the operator bias, induced by non-standardized and manual base line subtraction, (2) it is more precise and less time consuming than manual curve-fitting, especially for complex low temperature spectra with broad defect peaks. Furthermore, disturbing peaks of other mineral phases (i.e. carbonates or oxides) can be automatically subtracted so they do not affect the temperature estimation. Finally, each automatically generated curve-fit was quality-checked and low-quality fits were discarded for the final temperature estimation (summarized in Table DR2, see below).

Section DR2: RSCM data, sample information, and assumptions

RSCM results, associated errors, other key parameters and additional sample information are presented in Table DR2, together with existing RSCM data from literature used in this study. Samples were collected in a way so they are spatially distributed in horizontal and vertical direction along section trace X'X''. Sample elevation ranges from 935 m to 3070 m. Sample location data are shown in Table DR2. Samples M9, M22, M23, M24, M67 and M73 were collected and described by Menkveld (1995), samples 001, 002, 003 and 005 were taken from the sample collection situated at the Institute of Geological Sciences, University of Bern. Samples comprise both, carbonate-dominated shelf deposits and silicate dominated clastic sediments of Carboniferous to Cenozoic age (see Table DR2 for the stratigraphic units). The attribution of a stratigraphic unit given in Table DR2 is based on visual observations on outcrop, hand specimen and thin section scale. This was sometimes difficult, especially for strongly deformed and often completely recrystallized samples from the Windgällen-Färnigen and Urseren-Garvera zones.

In order to reduce potential biases arising from the presence of different types of CM in different stratigraphic units, we tried to sample the black shales (Mols-Member) situated at the base of the Middle Jurassic (Dollfuss, 1965) whenever possible. The effect of strain (Barzoi, 2015) or shear heating on the structural organization of CM has not been assessed in this study, but could potentially be a significant source of bias.

The temperature distribution of each sample was assessed in the form of a histogram (with a bin width of 10°C). Temperatures (RSCM-T) plotted in Table DR2 are mean values, where a near normal temperature distribution was observed. For samples with a bimodal or more complex

temperature distribution, we plotted the local maximum with the least temperature (i.e. samples FA-16-02, 003).

Table DR2: RSCM data, sample informations and locations

Sample number	Location			Tmax (°C)	SD (°C)	Error (°C)	N	Curve-fitting method	Stratigraphic unit	Tectonic unit	D1 (km)	D2 (km)	Reference
	Lat (°N)	Long (°E)	Elevation (m)										
SU-16-03	46.8348	8.5306	2310	224	17	40	15	Lu	Cenozoic	LH	44.6	1.79	This study
SU-16-04	46.8188	8.5132	1750	269	5	40	19	Lu	Cenozoic	LH	45.0	0.45	This study
EN-16-01	46.7926	8.4587	1250	265	12	40	18	Lu	Middle Jurassic	LH	46.7	0.05	This study
ER-15-16	46.8106	8.5523	1900	270	9	40	22	Lu	Middle Jurassic	LH	48.3	0.05	This study
WE-16-03	46.7604	8.4042	1970	283	10	40	22	Lu	Middle Jurassic	LH	49.4	0.05	This study
001	46.7703	8.4466	2640	295	4	40	4	Lu	Permo-Carboniferous	LH	49.8	-0.10	This study
002	46.7703	8.4466	2640	288	18	40	36	Lu	Permo-Carboniferous	LH	49.8	-0.10	This study
WE-16-02-2	46.7699	8.4442	2609	267	13	40	20	Lu	Triassic	LH	49.8	0.05	This study
KG-16-01	46.7825	8.5679	3070	274	5	40	16	Lu	Upper Jurassic	LH	51.5	0.08	This study
SE-15-05	46.7723	8.5380	2920	305	13	40	9	Lu	Middle Jurassic	LH	52.1	0.01	This study
FA-15-05	46.7303	8.4741	2540	345	24	40	24	Lu	Cenozoic	LH	55.0	0.15	This study
IN-15-06	46.7561	8.5906	2220	333	13	40	10	Lu	Permo-Carboniferous	LH	55.4	-0.30	This study
RB-15-02	46.7477	8.5511	2400	354	5	40	5	Lu	Middle Jurassic	LH	55.4	0.02	This study
FER-4	46.7359	8.5204	1450	326	11	40	14	Lu	Upper Jurassic	LH	55.5	0.01	This study
FA-15-13	46.7132	8.4481	2750	377	9	40	5	Lu	Permo-Carboniferous	LH	57.1	-0.30	This study
FA-16-02	46.7204	8.4626	2210	345*	25	40	28	Lu	Middle Jurassic	LH	57.1	0.05	This study
FA-15-21	46.7268	8.4826	2580	346	24	40	22	Lu	Middle Jurassic	LH	57.7	0.01	This study
FA-15-22b	46.7268	8.4827	2550	388	14	40	9	Lu	Permo-Carboniferous	LH	57.7	-0.01	This study
005	46.6759	8.3698	2300	439	32	40	56	Lu	Permo-Carboniferous	LH	64.2	-5.77	This study
003	46.6792	8.3779	2600	430*	27	40	23	Lu	Permo-Carboniferous	LH	64.6	-5.77	This study
UG13_6	46.5919	8.4696	2100	489	na	50	27	Be	Lower Jurassic	UGZ	83.0	0.30	Erne (2014)
UG13_5	46.5720	8.4119	2425	511	na	50	28	Be	Lower Jurassic	UGZ	83.5	0.25	Erne (2014)
UG13_8	46.6028	8.5049	1670	515	na	50	26	Be	Lower Jurassic	UGZ	83.5	0.30	Erne (2014)
UG13_10	46.6341	8.5989	1450	497	na	50	26	Be	Permo-Carboniferous	UGZ	84.8	0.25	Erne (2014)
Andermatt	46.6403	8.5945	1440	500	na	50	10-15	Be	Middle Jurassic	UGZ	84.8	0.20	Beyssac et al. (2002)
UG13_9	46.6410	8.5947	1480	517	na	50	27	Be	Upper Jurassic	UGZ	84.8	0.30	Erne (2014)
SU-16-01	46.8369	8.5317	2420	256	24	40	16	Lu	Lower Jurassic	HN	—	—	This study
SU-16-02	46.8365	8.5322	2350	275	12	40	21	Lu	Lower Jurassic	HN	—	—	This study
M9	46.7935	8.3941	1770	272	5	40	9	Lu	Lower Jurassic	HN	—	—	This study
M22	46.8315	8.3670	935	247	6	40	15	Lu	Middle Jurassic	HN	—	—	This study
M23	46.8193	8.4477	2000	286	11	40	14	Lu	Middle Jurassic	HN	—	—	This study
M24	46.8573	8.4500	2334	220	11	40	10	Lu	Middle Jurassic	HN	—	—	This study
M73	46.7831	8.3968	2230	270	5	40	16	Lu	Upper Jurassic	HN	—	—	This study
M67	46.7788	8.3944	2220	270	3	40	2	Lu	Cenozoic	HN	—	—	This study

Samples from this study are stored in the collections of the University of Bern, Institute of Geological Sciences, Switzerland. Tmax = RSCM peak temperature (Alpine), SD = standard deviation, Error = temperature calibration based error, N = number of considered spectra, D1 = present day true distance along top basement (=base Mesozoic), D2 = present day minimum distance to top basement (=base Mesozoic), Lu = Lünsdorf et al. (2017), Be = Beyssac et al.

(2002), LH = Lower Helvetic units, UGZ = Urseren-Garvera zone, HN = Upper Helvetic nappes, published temperature data from the UGZ are from Beyssac et al. (2002) and Erne (2014), * Based on a local maximum (bimodal or more complex temperature distribution).

Age of metamorphism recorded by RSCM

RSCM records peak metamorphic temperature regardless of the time when it was reached. In order to constrain the absolute age of peak metamorphism, independent constraints, for example from geochronology data, are needed. In this section, we discuss the age of obtained maximum temperatures, shown in Table DR2, and outline associated assumptions. The age of peak temperature quantified by RSCM is in most cases younger than the depositional age of the analyzed sediment. Exceptions are expected in clastic sediment associated with a high detrital input of CM of higher metamorphic grade. In the Central Alps, Mesozoic and younger samples have experienced Alpine metamorphism only, and are therefore likely to yield Alpine metamorphic peak temperatures. On the other hand, Permo-Carboniferous or older sediments could potentially be affected by contact metamorphism related to post-Variscan magmatic intrusions (e.g. Central Aar Granite, Franks, 1968a, 1968b; Labhart, 1977; Oberhänsli et al., 1988; Schaltegger and Corfu, 1995; Schenker, 1987; Schenker and Abrecht, 1987). We consider all RSCM peak temperatures shown in Table DR2 to represent Alpine peak metamorphic conditions. This assumption is supported by the fact that (1) adjacent samples of Carboniferous and Mesozoic age at two independent localities (Wendenjoch, Windgälllen-Färnigen zone) yield almost equivalent temperatures and (2) that all temperature estimates follow the same overall temperature trend, without major outliers, as seen on Fig. 2A. Temperatures of 500°C and higher were locally observed in single particles of CM, especially in pre-Mesozoic clastic sediments

(i.e. samples 003 and 005), but also in Mesozoic samples (FA-16-02). These might represent detrital input of higher grade metamorphic CM of pre-Alpine age.

Inferring that Alpine peak metamorphism was spatially isochronous along a cross-sectional distance of more than 40 km is a significant assumption (Wiederkehr et al., 2011). The age of peak Alpine metamorphism along the studied section is not completely resolved, especially in the external Aar Massif. This is mainly due to the low grade of metamorphism (greenschist to sub-greenschist facies) and due to the absence of suitable lithologies, minerals and grain sizes for present day dating methods. Furthermore, obtained isotopic ages on greenschist facies micas are often ambiguous and it remains controversial if such ages represent formation, cooling or mixed ages (e.g. Rolland et al., 2009).

Along cross-section X'X'' (Fig. 2C), most ages are reported from the Urseren-Garvera zone, a narrow zone containing the sedimentary cover of the Gotthard nappe (e.g. Bonanomi et al., 1992; Wyss, 1986, see also Section DR4). There, the metamorphic peak is dated at 17 - 21 Ma based on U-Th-Pb ages on allanite. The dated peak metamorphic allanite minerals overgrow the preexisting main Alpine foliation, indicating that in this zone, the thermal peak occurred relatively late with respect to deformation (Janots and Rubatto, 2014).

In the central southern Aar Massif the age of peak metamorphism is estimated at 17 - 22 Ma by Ar-Ar and K-Ar ages on micas (Berger et al., 2017; Challandes et al., 2008; Rolland et al., 2009).

In the external Aar Massif, the age of peak metamorphism is poorly constrained. Exposed poly-cyclic metamorphic basement units do not yield reliable Alpine ages (Berger et al., 2017). Alpine peak temperatures were not sufficiently high to reset thermochronometers such as the zircon fission track (ZFT) system. The lower age boundary is constrained by the northernmost and possibly Alpine reset ZFT cooling ages which cluster between 17 and 27 Ma (Michalski and

125 Soom, 1990; Wangenheim, 2016). Furthermore, retrograde hydrothermal monazites from an
126 Alpine cleft were dated at 13 - 17 Ma (Janots et al., 2012). The upper age boundary is
127 constrained by the Rupelian (28-34 Ma) age of flysch deposits (Matt Formation, e.g. Menkveld-
128 Gfeller et al., 2016), which represent the youngest sediment to be deposited onto the Aar massif
129 basement prior to its burial below the Helvetic and more internal Nappes.
130 Thermal calculations by Challandes et al. (2008) suggest that at least 10 Ma are required to heat
131 the Aar massif basement and its cover to its maximum temperature of 450°C, when
132 instantaneous burial and conductive thermal equilibration are assumed.
133 Although the age record is not very conclusive, we do not see clear indications of diachrony in
134 the published age data, as would be expected from an in sequence development. Rather, the data
135 are in favor of one spatially near-isochronous metamorphic peak at 17 to 22 Ma along the section
136 of consideration, between the Urseren-Garvera zone (parautochthonous Gotthard cover) in the
137 south and the external Lower Helvetic domain in the north.
138 The suggested age is in accordance with other stratigraphic and structural observations
139 (Burkhard, 1988), indicating that most of the crustal-thickening in the Aar Massif postdates the
140 emplacement of the Helvetic Nappes and higher tectonic units (Schmid et al., 1996).
141
142 **Geothermal gradient at peak temperature conditions**
143 For the tectonic reconstruction shown in Fig. 2C we assume a constant geothermal gradient of
144 25°C/km in the studied section at the time of peak metamorphism (17 - 22 Ma). Treating
145 isotherms as horizontal at a given time in a dynamic system such as the external central Alps is a
146 significant assumption, which will be discussed and justified in this section.

147 In a setting associated with rapid tectonic movements, heat advection towards or away from the
148 surface can produce oblique or locally even inverted thermal gradients (e.g. England and Molnar,
149 1993). Our top basement reference horizon is situated in the footwall of the basal Helvetic thrust,
150 where tectonic movements have taken place prior to and possibly also during the reference time
151 at 17-22 Ma (Schmid et al., 1996).
152 However, numeric models (Molnar and England, 1990; Shi and Wang, 1987) indicate that
153 thermal perturbations across an active thrust re-equilibrate relatively rapidly, especially for low-
154 angle thrusts with slip rates no higher than 5 mm/a, such as the basal Helvetic thrust,
155 representing the main active tectonic boundary at that time (Burkhard, 1988; Handy et al., 2010;
156 Schmid et al., 1996). Furthermore, the reference time chosen predates most of the Aar Massif
157 deformation and uplift. Apart from relatively slow tectonic burial in the footwall to the basal
158 Helvetic thrust, we do not expect significant vertical displacements along our reference horizon
159 at 17-22 Ma.
160 Therefore, although minor perturbations cannot be excluded or might even be expected, we
161 assume here an overall steady state geothermal gradient of 25°/km depth around peak
162 metamorphic conditions. This value is in agreement with independent pressure and temperature
163 estimates obtained on peak metamorphic mineral assemblages from the central southern Aar
164 Massif (Challandes et al., 2008; Goncalves et al., 2012) as well as with almost constant
165 metamorphic gradients along all major Helvetic thrusts (Ebert et al., 2008).
166

167 **Section DR3: Field data and projection**

168 This section contains supplementary information about the techniques and data that were used to
169 construct cross-section XX'' (Fig. 1A), with special emphasis on the geometry of the top

basement marker horizon. The tectono-metamorphic position of the Urseren-Garvera zone, situated in the very south of the studied cross-section will be discussed below (Section DR4). Permo-Carboniferous sediments occur only locally and are often restricted to graben-like structures. In this study, the term «top basement» strictly speaking refers to the base of the spatially inclusive Mesozoic sediments.

The Helvetic nappes are redrawn from an existing cross-section based on decades of field work and on reflection seismic data summarized in Pfiffner et al. (2011) and Pfiffner (2017). Below the Helvetic nappes, the geometry of top basement, including the Alpine sole thrust, is relatively well-constrained by strong reflectors in the autochthonous and par-autochthonous sediment cover (Pfiffner et al., 1997). For the Aar Massif domain of the studied section, we integrated existing geological surface data (Berger et al., 2016), unpublished subsurface data (hydropower galleries KW Wassen and Göschenen) and new field data from shear zone mapping along the transect. From a structural point of view, the position of the cross-section is ideal: top basement is exposed over a large distance as well as high relief and the easterly axial plunge of the Aar Massif (Hitz and Pfiffner, 1994) allows us to project higher tectonic levels into the profile, which significantly enlarges its vertical extent. Where eroded, the top basement geometry was projected into the profile from the East parallel to the average axial plunge of 070/10 (dipazimuth/dip). This value represents a cylindrical best fit, which is based on 227 field measurements of bedding as well as axes of early folds, measured in the par-autochthonous sediment cover of the eastern Aar Massif (Figure DR3). The same projection direction was used to project peak temperature data into section (Fig. 2B). Owing to structural complexity (i.e. non-cylindricity), a few (>10%) sample positions had to be adjusted by maximum a few hundred meters. Adjustments were made

192 only where necessary and with care so they do not significantly influence the resulting
193 temperature pattern and our interpretation.
194 The cross-section shown in Figs. 1A and 2B is line and area balanced. Constant line length was
195 assumed for the top basement horizon and constant area was assumed for the European crustal
196 basement. The present day area of the European crustal basement, especially its lower boundary
197 (Moho), is based on geophysical data (Wagner et al., 2012). The different degree of detail in
198 higher tectonic levels with respect to lower tectonic levels mostly reflects the different spatial
199 resolution of surface and geophysical data.
200 Mapped shear zones along the studied section are dominated by dip-slip kinematics. Shear zones
201 with oblique or strike-slip displacements have been reported, especially in the hinterland region,
202 but are considered to be of minor importance for the studied section in the eastern Aar Massif.
203 This is in contrast to the central and western Aar massif where a dense network of strike-slip
204 dominated shear zones is documented (Choukroune and Gapais, 1983; Rolland et al., 2009;
205 Steck, 1968; Wehrens et al., 2017). Although cross-section XX'' is oriented in the main
206 displacement direction, deformation was certainly not plane strain. Shear zones with oblique or
207 strike-slip and the corresponding displacements in or out of the section are not considered here.

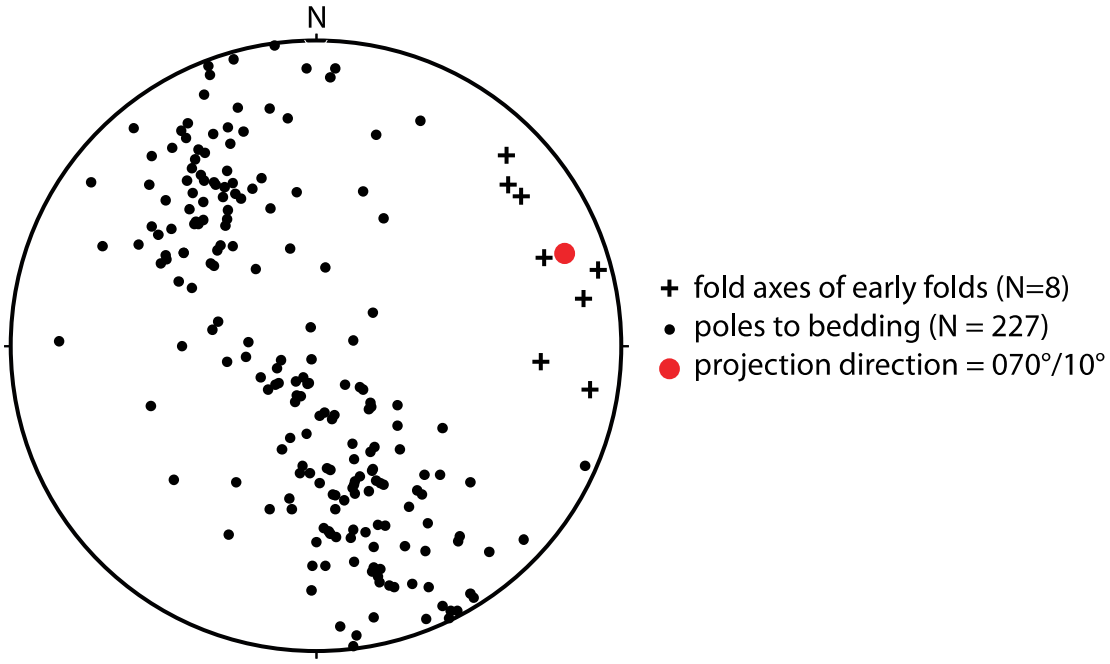

Figure DR3: Stereographic projection of poles to bedding and fold axes of early folds from the parautochthonous sediment cover of the eastern Aar Massif (Schmidt, lower hemisphere). The projection direction represents the pole to the great circle best fitting the poles of bedding (cylindrical best fit) and closely matches fold axes of early folds directly measured in the field. N = number of measurements.

Section DR4: Tectonometamorphic position of the Urseren-Garvera zone

On cross-section XX'' (Figs. 1A and 2B), the Urseren-Garvera zone is drawn as a tight upright syncline with a weakly developed northern limb and a much thicker southern limb. In the north, it is bound by an Alpine weakly reactivated Mesozoic south-vergent normal fault (Wyss, 1986). Stratigraphic polarity, large thickness of Lower Jurassic sediments and the absence of Middle Jurassic and younger sediments suggest that the Mesozoic and Permo-Carboniferous of the Urseren-Garvera zone represent the cover of the Gotthard Nappe (Bonanomi et al., 1992; Wyss, 1986).

In contrast, from a tectonic point of view, we assign the Urseren-Garvera zone to the footwall of the basal Helvetic thrust. As nicely documented in Wyss (1986) and indicated on Figs. 1A, 2B and 2C, the Urseren-Garvera zone represents the portion of the Gotthard nappe cover that has not been sheared off with the Helvetic nappes, but stayed attached to its crystalline substratum. This interpretation is consistent with almost equivalent metamorphic ages from the Urseren-Garvera zone and from the southern Aar Massif (see Section DR2) and justifies a comparison of RSCM peak temperatures obtained from the two different units in the form of isothermal contour lines (Figs. 1B and 2B).

REFERENCES CITED

Barzoi, S.C., 2015, Shear stress in the graphitization of carbonaceous matter during the low-grade metamorphism from the northern Parang Mountains (South Carpathians) - Implications to graphite geothermometry: International Journal of Coal Geology, v. 146, p. 179–187, doi: 10.1016/j.coal.2015.05.008.

Berger, A., Mercolli, I., Herwegh, M., and Gnos, E., 2016, Geological Map of the Aar Massif, Tavetsch and Gotthard Nappes: Geol. Spec. Map 129, Swisstopo, scale 1:100 000, 1 sheet.

Berger, A., Wehrens, P., Lanari, P., Zwingmann, H., and Herwegh, M., 2017, Microstructures, mineral chemistry and geochronology of white micas along a retrograde evolution: An example from the Aar massif (Central Alps, Switzerland): Tectonophysics, v. 721, p. 179–195, doi: 10.1016/j.tecto.2017.09.019.

Beyssac, O., Goffé, B., Chopin, C., and Rouzaud, J.N., 2002, Raman spectra of carbonaceous material in metasediments: A new geothermometer: Journal of Metamorphic Geology, v. 20, p. 859–871, doi: 10.1046/j.1525-1314.2002.00408.x.

Bonanomi, Y.-P., Dietler, T., and Etter, U., 1992, Querschnitt zwischen dem südlichsten Aar-Massiv und der Lucomagno-Decke im Bereich des Gotthard-Basistunnels: Eclogae Geologicae Helvetiae, v. 85, p. 257–266, doi: 10.5169/seals-167006.

Burkhard, M., 1988, L'Helvétique de la bordure occidentale du massif de l'Aar (évolution tectonique et métamorphique): Eclogae Geologicae Helvetiae, v. 81, p. 63–114, doi: http://dx.doi.org/10.5169/seals-166171.

Challandes, N., Marquer, D., and Villa, I.M., 2008, P-T-t modelling, fluid circulation, and 39Ar-40Ar and Rb-Sr mica ages in the Aar Massif shear zones (Swiss Alps): Swiss Journal of Geosciences, v. 101, p. 269–288, doi: 10.1007/s00015-008-1260-6.

Choukroune, P., and Gapais, D., 1983, Strain pattern in the Aar Granite (Central Alps): Orthogneiss developed by bulk inhomogeneous flattening: Journal of Structural Geology, v.

5, p. 411–418, doi: 10.1016/0191-8141(83)90027-5.
Dollfuss, S., 1965, Über den Helvetischen Dogger zwischen Linth und Rhein: Eclogae Geologicae Helvetiae, v. 58, p. 455–513, doi: 10.5169/seals-163277.
Ebert, A., Herwegh, M., Berger, A., and Pfiffner, A., 2008, Grain coarsening maps for polymineralic carbonate mylonites: A calibration based on data from different Helvetic nappes (Switzerland): Tectonophysics, v. 457, p. 128–142, doi: 10.1016/j.tecto.2008.05.007.
England, P., and Molnar, P., 1993, The interpretation of inverted metamorphic isograds using simple physical calculations: v. 12, p. 145–157.
Erne, S., 2014, Temperaturabschätzung der Metasedimente zwischen Gotthard- und Aar-Massiv in der Urseren-Garvera Zone, mittels Ramanspektroskopie [Bachelor Thesis]: University of Bern.
Franks, G., 1968a, A study of the Upper Palaeozoic Sediments and Volcanics in the Northern Part of the Eastern Aar Massif [Doctoral Thesis]: ETH Zürich, doi: https://doi.org/10.3929/ethz-a-000090580.
Franks, G., 1968b, The pre-Westphalian (Hercynian) metamorphism and structures of the Tödi Area (Aar massif): Schweiz. mineral. petrogr. mitt., v. 48, p. 667–694.
Goncalves, P., Oliot, E., Marquer, D., and Connolly, J.A.D., 2012, Role of chemical processes on shear zone formation: An example from the grimsel metagranodiorite (Aar massif, Central Alps): Journal of Metamorphic Geology, v. 30, p. 703–722, doi: 10.1111/j.1525-1314.2012.00991.x.
Handy, M.R., M. Schmid, S., Bousquet, R., Kissling, E., and Bernoulli, D., 2010, Reconciling plate-tectonic reconstructions of Alpine Tethys with the geological-geophysical record of spreading and subduction in the Alps: Earth-Science Reviews, v. 102, p. 121–158, doi: 10.1016/j.earscirev.2010.06.002.
Hitz, L., and Pfiffner, O.A., 1994, A 3d Crustal Model of the Eastern External Aar Massif Interpreted from a Network of Deep Seismic Profiles: Schweiz. mineral. petrogr. mitt., v. 74, p. 405–420, doi: 10.5169/seals-52086.
Janots, E., Berger, A., Gnos, E., Whitehouse, M., Lewin, E., and Pettke, T., 2012, Constraints on fl uid evolution during metamorphism from U – Th – Pb systematics in Alpine hydrothermal monazite: Chemical Geology, v. 326–327, p. 61–71, doi: 10.1016/j.chemgeo.2012.07.014.
Janots, E., and Rubatto, D., 2014, U-Th-Pb dating of collision in the external Alpine domains (Urseren zone, Switzerland) using low temperature allanite and monazite: Lithos, v. 184–187, p. 155–166, doi: 10.1016/j.lithos.2013.10.036.
Labhart, T.P., 1977, Aarmassiv und Gotthardmassiv: Gebr. Bornträger, Berlin-Stuttgart, Sammlung geol. Führer, 63, 173 p.
Lünsdorf, N.K., Dunkl, I., Schmidt, B.C., Rantitsch, G., and von Eynatten, H., 2014, Towards a Higher Comparability of Geothermometric Data obtained by Raman Spectroscopy of Carbonaceous Material. Part I: Evaluation of Biasing Factors: Geostandards and Geoanalytical Research, v. 38, p. 73–94, doi: 10.1111/j.1751-908X.2013.00249.x.
Lünsdorf, N.K., Dunkl, I., Schmidt, B.C., Rantitsch, G., and von Eynatten, H., 2017, Towards a Higher Comparability of Geothermometric Data Obtained by Raman Spectroscopy of Carbonaceous Material . Part 2 : A Revised Geothermometer: , p. 1–20, doi: 10.1111/ggr.12178.
Lünsdorf, N.K., and Lünsdorf, J.O., 2016, Evaluating Raman spectra of carbonaceous matter by

automated, iterative curve-fitting: International Journal of Coal Geology, v. 160–161, p. 51–62, doi: 10.1016/j.coal.2016.04.008.
Menkveld-Gfeller, U., Kempf, O., and Funk, H., 2016, Lithostratigraphic units of the Helvetic Palaeogene : review , new definition , new classification: Swiss Journal of Geosciences, v. 109, p. 171–199, doi: 10.1007/s00015-016-0217-4.
Menkveld, J.W., 1995, Der Bau des Helvetikums der Innerschweiz [Diploma Thesis]: Universität Bern.
Michalski, I., and Soom, M., 1990, The Alpine thermo-tectonic evolution of the Aar and Gotthard massifs, Central Switzerland - Fission Track ages on zircon and apatite and K-Ar mica ages: Schweiz. Mineral. Petrogr. Mitteilg, v. 70, p. 373–387, doi: 10.5169/seals-53628.
Molnar, P., and England, P., 1990, Temperatures, heat flux, and frictional stress near major thrust faults: Journal of Geophysical Research, v. 95, p. 4833–4856, doi: 10.1029/JB095iB04p04833.
Oberhänsli, R., Schenker, F., and Mercolli, I., 1988, Indications of Variscan nappe tectonics in the Aar Massif: Schweizerische Mineralogische und Petrographische Mitteilungen, v. 68, p. 509–520, doi: http://doi.org/10.5169/seals-52086.
Pfiffner, O.A., 2017, Thick-Skinned and Thin-Skinned Tectonics: A Global Perspective: Geosciences, v. 7, p. 71, doi: 10.3390/geosciences7030071.
Pfiffner, A., Burkhard, M., Hänni, R., Kammer, A., Kligfield, R., Mancktelow, N., Menkveld, J.-W., Ramsey, J.G., Schmid, S.M., and Zurbriggen, R., 2011, Structural Map of the Helvetic Zone of the Swiss Alps including Vorarlberg (Austria) and Haute Savoie (France): Geol. Spec. Map 128, Swisstopo, scale 1:100 000, 7 sheets, 10 plates.
Pfiffner, O.-A., Lehner, P., Heitzmann, P., Mueller, S., and Steck, A., 1997, Deep Structure of the Swiss Alps: Results of NRP 20: Basel, Birkhäuser.
Rolland, Y., Cox, S.F., and Corsini, M., 2009, Constraining deformation stages in brittle-ductile shear zones from combined field mapping and 40Ar/39Ar dating: The structural evolution of the Grimsel Pass area (Aar Massif, Swiss Alps): Journal of Structural Geology, v. 31, p. 1377–1394, doi: 10.1016/j.jsg.2009.08.003.
Schaltegger, U., and Corfu, F., 1995, Late Variscan “Basin and Range” magmatism and tectonics in the Central Alps: evidence from U-Pb geochronology: Geodinamica Acta, v. 8, p. 82–98, doi: 10.1080/09853111.1995.11105276.
Schenker, F., 1987, Hinweise für kompressive Tektonik während der Ablagerung von oberpaläozoischen Sedimenten und Vulkaniten im Aarmassiv: Bull. Ver. schweiz. Petroleum-Geol. u. - Ing., v. 53, doi: 10.5169/seals-210912.
Schenker, F., and Abrecht, J., 1987, Prä-aargranitische Anatexis, variszische Kontaktmetamorphose und alpidische Regionalmetamorphose im Oberhasli (zentrales Aarmassiv, Schweiz): Schweiz. mineral. petrogr. mitt., v. 67, p. 13–26, doi: 10.5169/seals-51584.
Schmid, S.M., Pfiffner, O.A., Froitzheim, N., Schonborn, G., and Kissling, E., 1996, Geophysical -geological transect and tectonic evolution of the Swiss-Italian Alps: Tectonics, v. 15, p. 1036–1064, doi: 10.1029/96TC00433.
Shi, Y., and Wang, C.Y., 1987, Two-dimensional modeling of the P-T-t paths of regional metamorphism in simple overthrust terrains: Geology, v. 15, p. 1048–1051, doi: 10.1130/0091-7613(1987)15<1048:TMOTPP>2.0.CO;2.
Steck, A., 1968, Die alpidischen Strukturen in den Zentralen Aaregranite des westlichen

Aarmassivs: Eclogae Geologicae Helvetiae, v. 61, p. 19–48, doi: 10.5169/seals-163584.
Wagner, M., Kissling, E., and Husen, S., 2012, Combining controlled-source seismology and local earthquake tomography to derive a 3-D crustal model of the western Alpine region: Geophysical Journal International, v. 191, p. 789–802, doi: 10.1111/j.1365-246X.2012.05655.x.
Wangenheim, C., 2016, Wangenheim, Cornelia. Quantifying Fluvial and Glacial Erosion Using (detrital) Thermochronology, Cosmogenic Nuclides and Numerical Modelling: A Case Study in the European Alps [Doctoral Thesis]: Gottfried Wilhelm Leibniz Universität Hannover.
Wehrens, P., Baumberger, R., Berger, A., and Herwegh, M., 2017, How is strain localized in a meta-granitoid, mid-crustal basement section? Spatial distribution of deformation in the central Aar massif (Switzerland): Journal of Structural Geology, v. 94, p. 47–67, doi: 10.1016/j.jsg.2016.11.004.
Wiederkehr, M., Bousquet, R., Ziemann, M.A., Berger, A., and Schmid, S.M., 2011, 3-D assessment of peak-metamorphic conditions by Raman spectroscopy of carbonaceous material: An example from the margin of the Lepontine dome (Swiss Central Alps): v. 100, 1029-1063 p., doi: 10.1007/s00531-010-0622-2.
Wyss, R., 1986, Die Urseren-Zone: Lithostratigraphie und Tektonik: Eclogae Geol.Helv., v. 79, p. 731–767, doi: 10.5169/seals-165849.